SAND2018-4843J

Average neutron time-of-flight instrument response function inferred from single D-T neutron events within a plastic scintillator [a)]

J. D. Styron[1b)], C. L. Ruiz[2], K. D. Hahn[2], G. W. Cooper[1], G. A. Chandler[2], B. Jones[2], B. R. McWatters[2], C. J. Forrest[3], J. Vaughan[1], J. Torres[2], S. Pelka[1], J. Smith[2], C. Weaver[1]

[1]*Department of Nuclear Engineering, University of New Mexico, Albuquerque, NM 87131, USA*
[2]*Sandia National Laboratories, Albuquerque, NM 87123, USA*
[3]*Laboratory for Laser Energetics, University of Rochester, Rochester, New York 14623-1299, USA*

(Presented XXXXX; received XXXXX; accepted XXXXX; published online XXXXX)

The apparent ion temperature and neutron-reaction history are important characteristics of a fusion plasma. Extracting these quantities from a measured neutron-time-of-flight (nTOF) signal, either by convolution or de-convolution methods, requires accurate knowledge of the instrument response function (IRF). This work describes a novel method for obtaining the IRF directly for single DT neutron interactions by utilizing n-alpha coincidence. The t(d, α)n nuclear reaction was produced at Sandia National Laboratories' Ion Beam Laboratory using a 300-keV Cockcroft-Walton generator to accelerate a 2.5-μA beam of 175-keV D^+ ions into a stationary ErT_2 target. The average neutron IRF was calculated by taking a time-corrected average of individual neutron events within an EJ-228 plastic scintillator. The scintillator was independently coupled to two photo-multiplier tubes operated in current mode: a Hamamatsu 5946 mod-5 and a Photek PMT240. The experimental setup and results will be discussed.
Work supported by DOE NNSA contract DE-NA0003525.

I. Introduction

At Sandia National Laboratories' Z-Machine, the MagLIF (Magnetized Liner Inertial Fusion) concept is presently being studied as a fusion source.[1-2] Extensive x-ray and nuclear diagnostic suites are fielded on these experiments to ascertain several physics parameters relevant to understanding the implosion.[3-10] Several of these parameters can be inferred from data collected on several neutron time-of-flight (nTOF) detectors that view the plasma column through varying geometries, distances, and angles. For MagLIF experiments, we use NTOF diagnostics to infer the apparent ion temperature, degree of fuel magnetization, and beryllium liner areal density at stagnation.[11-15] To infer these quantities, we use a forward-fit (or convolution) model to compare with the measured data.[16] For each detector, this method requires obtaining the primary and down-scattered components of the neutron fluence from a set of expected source conditions (i.e., ion temperature and liner areal density) and, secondly, knowing the instrument response function (IRF)[17].

Historically, short-pulse x-ray sources, cosmic rays, or laser illumination have been used as a neutron surrogate to characterize the IRF for nTOF detector systems.[18, 19] Previous attempts have been made to generate IRFs directly from neutrons. Time-correlated single photon counting techniques have been studied using neutrons produced from accelerator-driven nuclear reactions.[20,21] Another technique is to approximate a single neutron interaction by placing the detector at a large distance from the source to minimize the number of neutrons incident on the detector from a pulsed neutron source.[22] To date, there are not adequate data that show the direct comparison of an IRF obtained directly from a neutron source and one produced from other sources (x rays, cosmic rays, etc.) for the same detector system. It is important to recognize that there are fundamental differences in the scintillation process that are charged-particle-specie dependent that may result in slight or subtle differences between neutron- and photon-induced IRFs that have not yet been resolved[23].

The majority of IRFs that are presently utilized in the analysis of nTOF data at the Z-Machine were measured in 2007 using 5-MeV x-rays produced at the Idaho State University Linear Accelerator. While these measurements provided a suitable IRF model at the time, newer nTOF detector systems with faster photomultiplier tubes (PMT) and different scintillators are being developed for Z experiments. Furthermore, the impulse response functions of the older, quenched detectors at Z may well have changed over the intervening ten years due to the potential degradation of the quenching mechanism. Thus, to ensure

[a)] Published as part of the Proceedings of the 22nd Topical Conference on High-Temperature Plasma Diagnostics (HTPD 2018) in San Diego, California, USA.
[b)]Author to whom correspondence should be addressed: jdstyro@sandia.gov.

the physics parameters inferred from the data are accurate, we need IRFs for the new and old nTOF detectors and the ability to monitor the IRFs over time (especially for the quenched scintillators).

To address the potential concern with non-neutron IRFs, we have developed a novel method of measuring the IRF directly from single DT neutron interactions. This technique can be applied to our new and older detectors and allows us to monitor the IRFs over their lifetime. This paper will describe the new dual PMT nTOF designs that are being implemented at the Z-machine, the experimental setup and the technique for measuring the IRF. We also discuss the experimental results, analysis, and plans for future work.

II. Dual-PMT nTOF detector

The neutron diagnostic team at the Z-Machine is in the process of replacing older nTOF systems with new, dual-PMT nTOF detectors. This new design, as shown in FIG. 1, allows data to be collected over a large dynamic range. One of the goals is to measure both the primary DD neutron signal and the very small secondary DT neutron signal from the same detector, and more importantly, in the same line-of-sight. This design utilizes a cylindrical plastic scintillator that is 2.54-cm thick with a 7.62-cm diameter. The scintillator is viewed through the edge, on opposing sides, by two, independently operated PMTs: a Hamamatsu 5946 mod-5 and a Photek PMT-240. The PMTs are coupled to the scintillator using 15.7 cm long, cone shaped, Lucite light-guides. The Hamamatsu PMT is the legacy PMT that has been fielded for decades at the Z-Machine and the Photek PMT-240 was chosen for its micro-channel plate design that has a time response that is ~3x faster than that of the Hamamatsu[24]. We are investigating two different scintillators which may be more suited for either the primary DD signal or the secondary DT signal. These include EJ-2332Q-1% (BC-422Q-1% eq.) and EJ-228 (BC-418 eq.) which is ~ 4X slower than EJ-232Q-1%, but produces ~ 7X more visible light output[25]. For the work presented here, a dual-PMT design was configured with EJ-228, as denoted in FIG. 1.

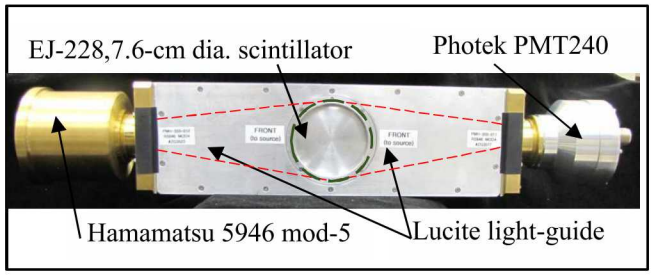

FIG. 1 Dual-PMT neutron time-of-flight detector.

III. Experimental geometry and reaction kinematics

DT neutrons from the t(d,α)n nuclear reaction were produced at Sandia National Laboratories' Ion Beam Laboratory (IBL) using a 300-keV Cockcroft-Walton generator to accelerate a 2.5-μA beam of 175-keV D^+ ions onto a stationary, 2.6-μm thick, ErT_2 target. Attached to the target chamber, 30.5-cm from the source, at fixed angles of 110^0 and 165^0 with respect to the beam, are two surface-barrier detectors (SBD) to measure the alpha particles produced in the reaction. The line-of-sight for each of the SBDs has a 2.6-μm thick aluminum foil to range out any Rutherford scattered deuterons and a 2.5-mm diameter collimator such that the solid angle (54 +/- 2 μsr) subtended by each detector geometry is very well defined. The number of alpha particles detected at either angle can be used, independently, to calculate the number of neutrons emitted into any angle using the Associated Particle Method (APM)[26]. For these experiments, we only required use of the 110^0 detector. The relevant components of the experimental configuration along with the nTOF detector under study are shown in FIG. 2.

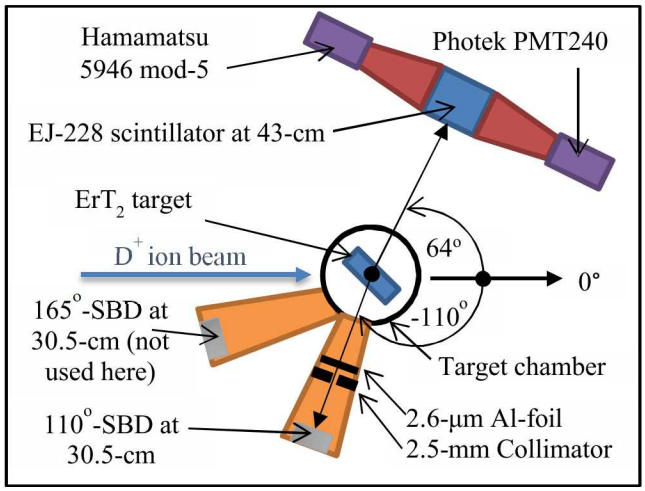

FIG. 2 Schematic of the 300-keV Cockroft-Walton target area, shown are the two charged particle detectors at 110^0 and 165^0 and the nTOF detector under study at 64^0.

The t(d,α)n reaction as it occurs in this configuration can be described using relativistic two-body kinematics (See Ref. 27 for equations). Using this formulation, the neutron angular distribution was calculated exactly for a fixed alpha emission into 110^0. The corresponding neutrons vary in angle and energy due to the change of center-of-mass motion associated with the dE/dx losses of the D^+ ion in the target material. At the initial ion energy, a reaction will occur near the front of the target which produces a 14.5 MeV neutron that is emitted at 61^0. Likewise, when the ion is fully ranged in the target, a reaction will occur at near 0-keV, which produces a 14.0 MeV neutron at 70^0. These relationships are depicted in FIG. 3 along with the range of expected flight-times. The nTOF detector, as shown in FIG. 1, was placed at 43.6 cm from the source at an angle of 64 +/- 5 degrees with respect to the beam to subtend a large enough solid-angle to measure all possible coincident events. The offset in angle is to account for more reactions occurring near the front of the target since the total DT fusion cross-section is higher at 175 keV. If a nearly mono-

energetic neutron energy is desired, the detector can be moved further away from the target or collimated to subtend a reduced solid angle.

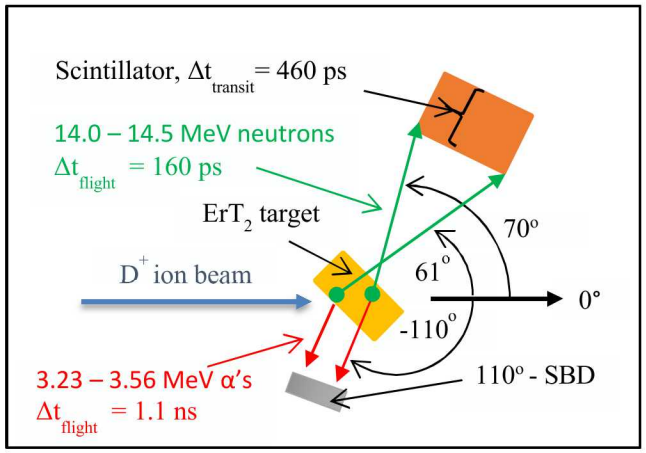

FIG. 3 Relevant kinematics for the t(d,α)n nuclear reaction for D^+ ion energies ranging from 0 – 175 keV and an alpha emission angle of 110^0 with respect to an incident 175-keV D+ beam.

IV. Data acquisition

The data acquisition system was designed to simultaneously measure electronic signals from the 110^0 SBD and the nTOF detector to establish that a single-event neutron interaction occurred within the scintillator. The outputs from both detectors were passed through 36.6-m of low-loss, 50-ohm, LMR-600 coaxial cables from the target area to the data acquisition center into separate Ortec-584 constant-fraction-discriminator (CFD) modules. The CFD units have adjustable lower-level-discriminators (LLD) and three available outputs that were used to monitor different quantities in this experiment. The 800-mV, adjustable-width, negative TTL-block (BK) output was used to monitor single-event count rates for both the SBD and nTOF detector at a prescribed LLD setting. One of the two available 800-mV, 5-ns, Gaussian-shaped negative-timing pulses from each CFD were input into a time-to-amplitude converter (TAC), with the nTOF and SBD outputs used to start and stop the data acquisition, respectively. The output from the TAC was analyzed using multi-channel-analyzer software (Ortec- Easy MCA) to produce a differential time-spectrum. Primarily this was used to determine the cable-length required to establish coincidence, but secondly, to serve as a visual coincidence rate monitor. The second timing output from each CFD was input into an Ortec 4020C logic unit. Prior to the logic unit, the nTOF CFD output was delayed using an Ortec 425A cable delay. The nominal delay required to establish particle coincidence was ~ 54 ns for the Hamamatsu-mod 5 and ~ 63 ns for the Photek-PMT240. The fast, negative timing output from the 4020C was routed through a counter to monitor the coincident count rates and the positive TTL output was used to trigger data acquisition on the Tektronix DPO7254C oscilloscope. Other electronics were included to monitor the differential energy spectrum of the alpha particles and the beam current as a function of time. These two systems, together, provide information about the time-dependent conditions of the target. A block diagram illustrating the relevant electronics used to establish coincidence and acquire the neutron IRF are shown in FIG. 4. The electronics used to monitor the alpha particle energy spectrum and the beam current are omitted here, but are discussed in detail in Ref. 26.

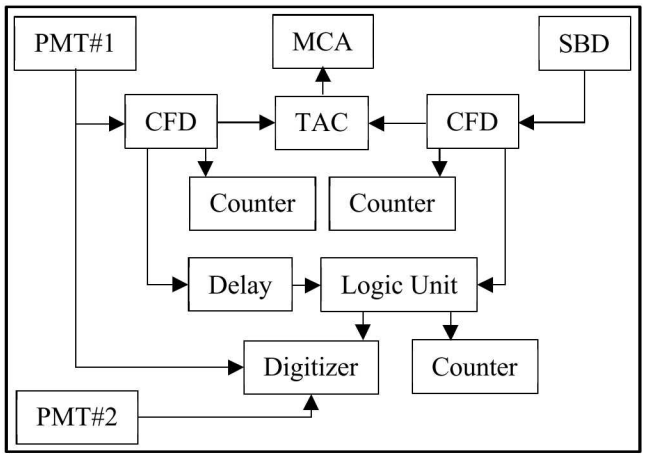

FIG. 4 Data acquisition system to measure and record the instrument response function and particle coincidence.

For each coincident event measured, the resulting neutron signals from both PMTs were recorded and saved on the oscilloscope over an 80-ns interval with 50-ps time resolution at a bandwidth of 2.5 GHz. At least 1000 nToF signals were collected for both PMTs as a function of the applied voltage to achieve a 3% uncertainty in the sampling statistics. With knowledge of the fixed delay between the two PMTs, at specific bias settings, the second PMT could be placed in coincidence during post-processing of the data. Measurements were repeated for each PMT being placed in coincidence with the 110^0 SBD at multiple bias settings. The applied voltage for the Hamamatsu PMT mod-5 was varied from -1.7 to -2.4 kV and the Photek PMT240 was varied from -3.8 kV to -4.6 kV; both in 0.1 kV increments. The lower limit on the applied voltage for each PMT is where the observed amplitude of the waveform approached 8 mV, which is the lowest discriminator level setting on the CFD-unit. The discriminator level for the PMT was adjusted for each bias setting to be just above the background level and the discriminator level for the SBD was fixed at 15 mV, which corresponds to the lower limit of the alpha energy spectrum.

V. Results – Particle coincidence

A typical coincidence curve that shows the differential time history between the measurement of the alpha particle and the neutron is shown in FIG. 5. The coincidence efficiency is 99.2% (counts within the peak/total counts), which leaves an inherent background of random incidentals of only 0.8%. The measured FWHM of the coincidence curve agrees with

the variable timing calculated from the kinematics, which is 1.72 ns. This is the sum of the variable timing associated with the time-of-flight for each particle (1.1 ns for the alpha and 0.16 ns for the neutron) and 0.46 ns for the neutron transit time through the scintillator. In addition, the number of neutrons inferred using the associated particle method suggests that there were nominally 1E5 neutrons per second incident on the detector for the stated conditions, or a neutron incident every 10 μs. This suggests that the probability of measuring multiple neutrons within the 80-ns acquisition interval was of minimal concern. Furthermore, if the nTOF detector is placed in anti-coincidence with the SBD detector (at an angle less than 61^0 or at an angle greater than 70^0 with respect to the beam) a constant count rate comparable to the random incidental rate was observed with no discernible peak region. Observing the anti-coincidence and the high coincidence efficiency further validates that the measured waveforms are indeed from DT neutrons interacting with the scintillator.

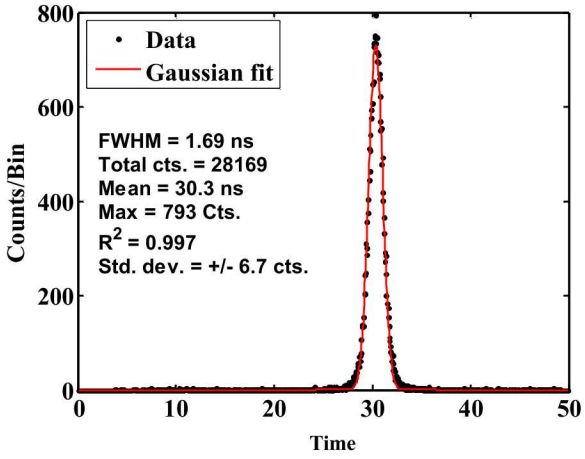

FIG. 5 Typical coincidence curve showing the time difference between the detection of the neutron and alpha particle from the same reaction.

VI. Results – Average instrument response function

Within this measurement there are several processes occurring that are highly statistical in nature. First, the probability of a neutron interacting within the scintillator is defined by an exponential probability distribution that is defined by the corresponding neutron mean-free-path of the scintillator. Once an elastic scattering interaction occurs there is a probability that the neutron will produce a recoil proton with an energy range from near zero to the full energy of the neutron as determined from reaction kinematics. Once the proton is produced, there is a probability that it will interact within the scintillator and produce an amount of visible light proportional to dE/dx[28]. The population and decay of scintillation states, the photocathode efficiency, and electron multiplication are all statistical processes that occur within the scintillator and PMT. Thus, it is pertinent for this measurement that we define a parameter that captures the mean probability of all these processes, or the average IRF.

While waveforms produced from single neutron interactions within the scintillator were measured for both the Hamamatsu mod-5 and the Photek PMT240, only the data taken at -4.0 kV with the Photek PMT240 is shown to emphasize the analysis technique. Seven waveforms are shown in FIG. 6 to illustrate the range of acquired data. On average, there were five observable structures within a single data acquisition for the Photek. These secondary structures are most likely caused by delayed phosphorescence in the scintillator through an increase in triplet-state production and not multiple neutron collisions, which will occur on a time-scale much less than the resolving time of the PMT. In addition, the change in amplitude is attributed to the energy carried by the elastically scattered proton, which can vary from near zero to the full energy of the neutron.

The average IRF was found by first normalizing each waveform to the leading edge at 10% of the maximum amplitude, and then averaging point-by-point over all measured waveforms. The variable leading edge was chosen to mitigate the transit time associated with the variable kinematics. It is also consistent with the properties of a Gaussian function, where the shape of the curve is the same regardless of the amplitude or area, thus making the analysis of this data insensitive to the applied normalization. This is demonstrated in FIG. 6 (right side), which shows the original seven waveforms (FIG. 6, left side) after the normalization has been applied.

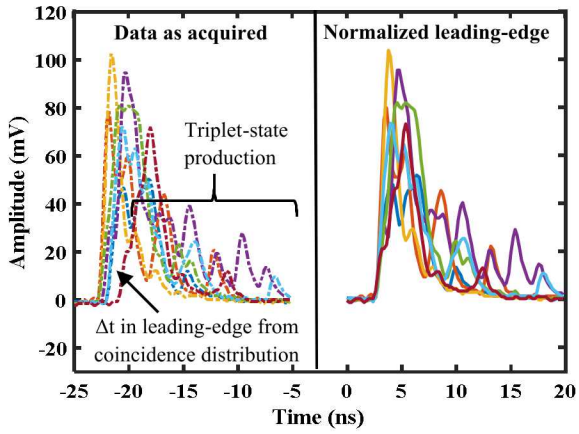

FIG. 6 Seven waveforms are shown for the Photek (-4.0 kV) PMT as acquired (left side) and after the leading-edge normalization was applied (right side). Data shifted in time for clarity.

On average, 99% of the acquired waveforms were used in the average analysis. Data not included in the analysis were rejected for having anomalous behavior, such as visible pre-pulses, reflections, or digitizer clipping. The averaged waveforms were fit using a Gaussian function convolved with an exponential decay (as shown in equation 1) to provide a functional description of the IRF. This function is non-linear with four unknown parameters: the centroid location (μ), the decay parameter (τ), the Gaussian width parameter (σ), and the amplitude (A). These

parameters were determined using a non-linear routine that utilized the Matlab® function <fminsearch> to iterate over the phase space until the variance between the fit and the average waveform were minimized and converged using the Nelder-Smead method[29].

$$IRF(t,\mu,\tau,\sigma,A) = A * \exp\left(-\frac{t-\mu}{\tau}\right)\exp\left(\frac{\sigma^2}{2\tau^2}\right)\left(1+\operatorname{erf}\left(\frac{t-\mu-\frac{\sigma^2}{\tau}}{\sqrt{2\sigma^2}}\right)\right) \quad (1)$$

An example of the entire process is depicted graphically in FIG. 7 for data taken with the Photek PMT240 at -4.0 kV. At least 1000 data acquisitions were normalized (black trace), averaged (magenta trace) and fit using the IRF model given in equation 1 (green trace). The values quoted in FIG. 7 correspond to the full-width at half-maximum (FWHM) of the IRF, the Gaussian FWHM, the decay parameter, the average charge deposited, and the R-squared and standard deviation of the fit.

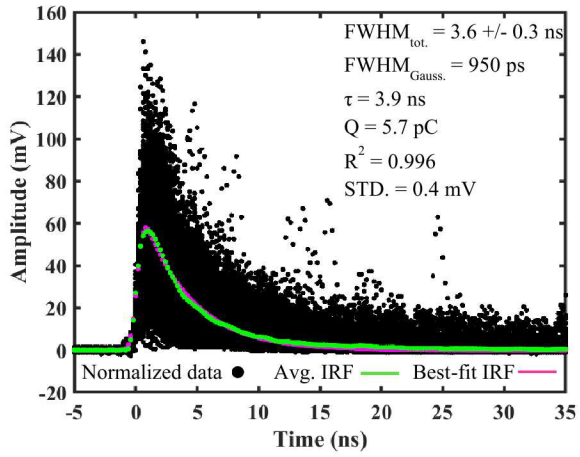

Fig. 7 Shown are the normalized data, the average IRF, and the functional fit for the Photek PMT240 at -4.0 kV.

The uncertainty for this analysis is very much a work in progress, but at present it is only defined for the FWHM of the signal, since providing uncertainty for each parameter requires work that is currently outside the scope of this paper. The uncertainty in the width was determined at the one-sigma level by taking the quadrature sum of the uncertainty associated with the leading-edge time value used to normalize the waveforms (which is consistent with the sum of the scintillator and neutron transit times) and the resolution of the measurement. This method produces a nominal uncertainty in the width of 300 ps. Statistical uncertainties from the averaging of amplitudes were assumed negligible due to the large number of data points that were averaged.

VII. SUMMARY AND FUTURE WORK

An average IRF was obtained for a current-integrated nTOF detector by acquiring waveforms that were produced from single DT neutron interactions within EJ-228 plastic scintillator. The values obtained for the IRF are expected for the PMTs and scintillator tested. Plans to compare IRFs obtained in this work to IRFs obtained with an x-ray source produced at OMEGA, for the same detector, are underway. Additional experiments at the IBL are planned later this year to show equivalency between DT and DD neutron induced IRFs. In addition, these measurements will be duplicated with EJ-232Q-1% quenched scintillator to show the reduction in triplet-state production.

VIII. ACKNOWLEDGMENTS

Sandia National Laboratories is a multimission laboratory managed and operated by National Technology and Engineering Solutions of Sandia, LLC., a wholly owned subsidiary of Honeywell International, Inc., for the U.S. Department of Energy's National Nuclear Security Administration under contract DE-NA-0003525. The views expressed in the article do not necessarily represent the views of the U.S. Department of Energy or the United States Government.

IX. REFERENCES

[1]S. A. Slutz *et al*, Phys. Plasmas **21**, (2014).
[3]M. R. Gomez *et al*, Phys. Rev. Lett. **113**, (2014).
[4]S. B. Hansen, *et al*, Phys. Plasmas **22**, 05613, (2015).
[5]K. D. Hahn, *et al*, J. Appl. Phys. **717**, (2016).
[6]C. L. Ruiz *et al*, Rev. Sci. Instrum. **63**, 4889, (1992).
[7]K. D. Hahn *et al.*, Rev. Sci. Instrum. **83**, 10D914, (2012).
[8]K. D. Hahn *et al*, Rev. Sci. Instrum. **85**, 043507, (2014).
[9]D. Ampleford *et al,* (These proceedings).
[10]J. Vaughan *et al*, (These proceedings).
[11]R.A. Lerche *et al*, Appl. Phys. Lett. **31**, 645 (1977).
[12]C. L. Ruiz *et al*, Phys. Rev. Lett. **93**, 015001 (2004).
[13]P. F. Schmit et al, Phys. Rev. Lett. **113**, (2014).
[14]M. R. Gomez *et al*, Phys. Plasmas **22**, 056306, (2015).
[15]P. F. Knapp *et al*, Phys. Plasmas **22**, 056312, (2015).
[16]T. J. Murphy *et al*, Rev. of Sci. Instrum. **68**, 610 (1997).
[17]A.J. Nelson *et al*, Rev. Sci. Instrum. **83**, (2012).
[18]R. Hatarik *et al*, J. Appl. Phys. **118**, 184502 (2015).
[19]M. A. Bonura *et al*, Rev. Sci. Instrum. **85**, 11D633 (2014).
[20]R. Hatarik *et al*, Rev. Sci. Instrum. **83**, 10D911 (2012).
[21]J. A. Brown *et al*, J. Appl. Phys. **115**, 193504 (2014).
[22]D. Klir, *et al*, Rev. Sci. Instrum. **82**, 033505 (2011).
[23]G. F. Knoll, "Radiation Detection and Measurement", 4th edition, New York: Wiley, (2010).
[24]Photek, http://www.photek.com/pdf/datasheets/
[25]Eljen Technologies, http://eljentechnology.com/products/
[26]C. L. Ruiz *et al*, Rev. Sci. Instrum. **83**, 10D913, (2012).
[27]Brookhaven National Laboratory, ENDF-6 Formats Manual, www.nndc.bnl.gov, (2012).
[28]J.B. Birks, The Theory and Practice of Scintillation Counting, Oxford: Pergamon Press, (1964).
[29]Lagarias *et al*, SIAM Journal of Optimization **8**, (1998).